J. Fluid Mech. (1990), *vol.* 211, *pp.* 95–122
Printed in Great Britain

Experimental investigation of three-dimensional turbulent boundary layers on 'infinite' swept curved wings

By V. BASKARAN†, Y. G. PONTIKIS‡ AND P. BRADSHAW‖
Department of Aeronautics, Imperial College of Science & Technology, London SW7 2BY, UK

(Received 27 July 1988 and in revised form 17 July 1989)

Mean flow and turbulence measurements have been made in three-dimensional turbulent boundary layers in curved ducts, simulating adverse pressure gradients on two 'infinite' swept curved wing surfaces with concave and convex curvature respectively. The ratio of the initial boundary-layer thickness to the surface radius of curvature in both cases is approximately 0.01, the value used in the earlier two-dimensional turbulent boundary-layer studies on the effects of concave and convex curvature by Hoffmann, Muck & Bradshaw (1985) and Muck, Hoffmann & Bradshaw (1985) respectively. The pressure-driven crossflow has nearly the same streamwise distribution as in the 'infinite' swept flat-surface experiment of Bradshaw & Pontikos (1985), which used a similar duct. The results of the present study show that the coupled effects of mean flow three-dimensionality and prolonged mild surface curvature of either sign have rather a weak influence on the turbulence structure, unlike the significant influence of the above extra strain rates when applied individually. In the concave case, the effect of the crossflow appears to oppose the destabilizing effect of curvature in addition to suppressing spanwise wavy inhomogeneities In contrast, the weak combined influence of convex curvature and crossflow, both of which, separately, tend to attenuate turbulence, implies that the interaction between the two effects is grossly nonlinear. Implications of the present results for turbulence modelling are briefly discussed.

1. Introduction

Many common turbulent shear layers suffer from the effects of rates of strain additional to simple shearing, or from interaction with another turbulent flow field. A complex flow of this kind is a shear layer with a cross-stream mean shear, $\partial W/\partial y$, as an extra strain rate, in addition to the basic component, $\partial U/\partial y$; it is commonly known as a 'three-dimensional boundary layer'. Typical examples are the flow over a swept wing, flow in turbomachine boundary layers, and flow through arbitrarily curved ducts or passages. In this type of flow, the x-component of mean vorticity is nearly equal to the cross-stream shear, $\partial W/\partial y$ (in the present paper we use y for the distance normal to the surface and z for the distance in the spanwise direction – see figure 1 – with V and W for the respective mean velocity components and Q for the resultant velocity magnitude). There is another type of three-dimensional flow, with imbedded vortices, such as in a wing-body junction, where $\partial V/\partial z \approx \partial W/\partial y$, and the

† Present address: Aeronautical Research Laboratories, DSTO Salisbury, Australia.
‡ Present address: British Aerospace Dynamics, Hatfield, Herts, UK.
‖ Present address: Thermosciences Division, Mechanical Engineering Dept, Stanford University, Stanford, CA 94305, USA.

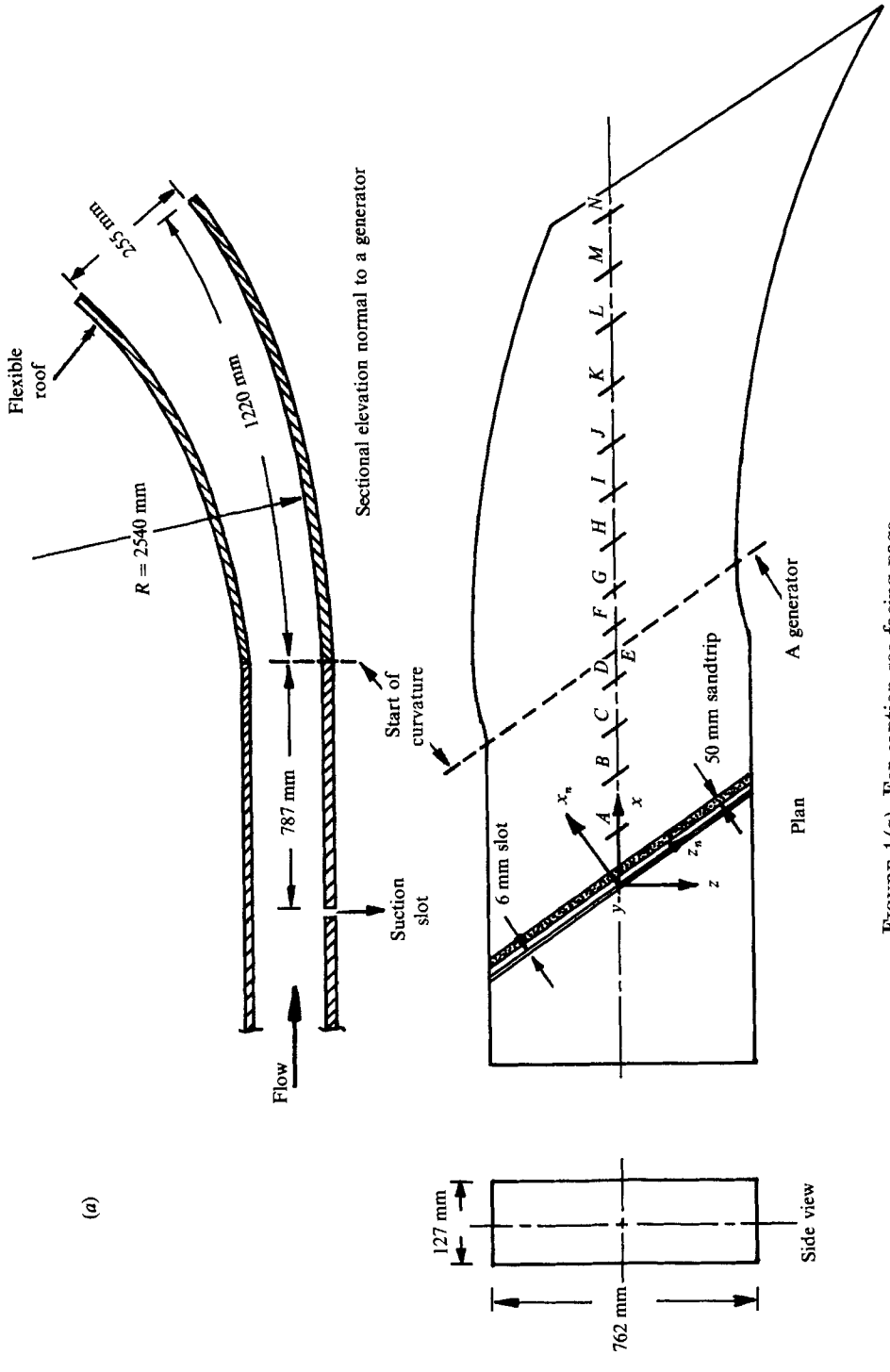

FIGURE 1(*a*). For caption see facing page.

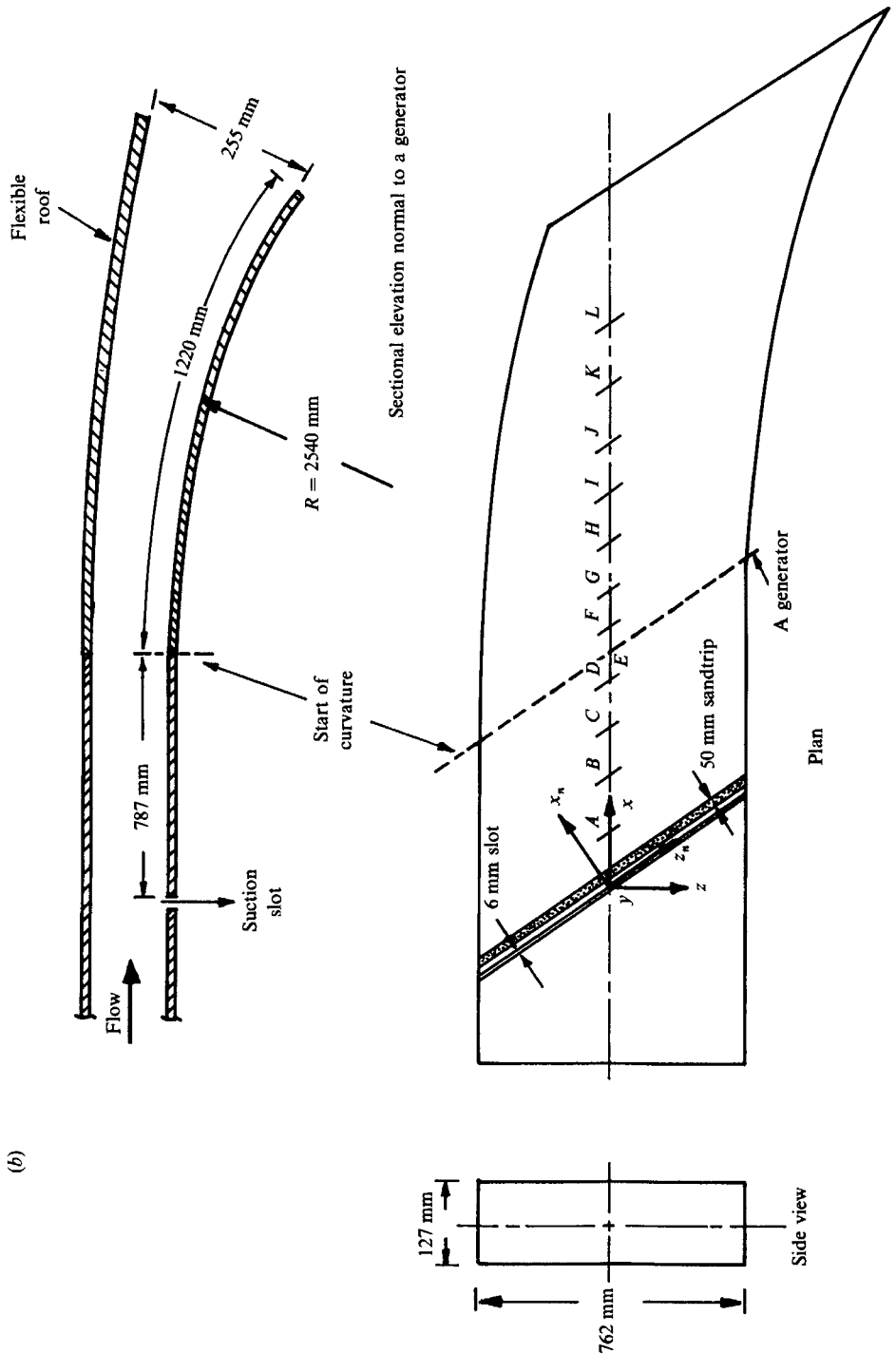

FIGURE 1. 35° swept curved wings. (*a*) Concave curvature rig. (*b*) Convex curvature rig.

two contribute roughly equally to the x-component of mean vorticity: a more detailed account of this type is given in Bradshaw (1987). This paper deals with the former type of three-dimensional flow, particularly that over 'infinite' swept wings†, in cases where longitudinal streamline curvature produces yet another extra strain-rate, $\partial V/\partial x$. Here 'longitudinal' is used, following Bushnell & McGinley (1989) to distinguish streamline curvature, as seen in spanwise view, from lateral curvature (seen in front view) or crossflow curvature (as seen in plan view). Crossflow or plan-view curvature is the essential feature of three-dimensional boundary layers, seen even on a flat surface. It is easy to distinguish plan-view curvature from that in any plane normal to the surface, but so little is understood about curvature effects in three-dimensional boundary layers that it is not clear which normal plane defines the curvature that affects the turbulence. The most plausible simple guess, used in the calculations presented below is the component in the plane of the resultant shear stress $(-\overline{uv}, -\overline{vw})$. Streamline curvature within the flow differs significantly from surface curvature if the rate of growth of the boundary layer is changing rapidly, but consideration of a local value at each y is simplistic, since curvature mainly affects the large eddies. In the present 'infinite wing' case, any choice for the effective curvature can be evaluated from the principal surface curvature (in the plane normal to the generators). Note that the crossflow extra strain rate, $\partial W/\partial y$, specifies streamwise mean vorticity, while the curvature extra strain rate, $\partial V/\partial x$, affects the spanwise mean vorticity. In this paper, we address the combined effects of crossflow and streamline curvature on the turbulence structure. By 'structure' we mean the empirical information that normally links experiments and engineering calculation methods, where it appears as (allegedly constant) dimensionless parameters such as the ratio of shear stress to turbulent kinetic energy.

The present investigation is one in a series of complex flows studied at Imperial College, and is specifically a sequel to the study of Bradshaw & Pontikos (1985) on a three-dimensional turbulent boundary layer. This work in turn was a repeat and extension of the experimental work at the Netherlands NLR by van den Berg *et al.* (1975) and by Elsenaar & Boelsma (1974), on the flow in a duct simulating an 'infinite' swept wing. In both cases the leading-edge sweep was 35°, and the 'infinite' swept conditions were simulated by shaping the sidewalls of a finite-width test section. The principal conclusion of the study of Bradshaw & Pontikos is that the turbulent activity in a three-dimensional boundary layer (as measured by the eddy viscosity or by the resultant shear stress/turbulent energy ratio) is considerably less than in two-dimensional boundary layers. In an earlier phase of the investigations into complex flows at Imperial College, the effect of mild prolonged longitudinal streamline curvature on two-dimensional boundary layers was studied in detail. Concave and convex curvature was considered by Hoffmann *et al.* (1985) and Muck *et al.* (1985) respectively. The surface radius of curvature was approximately 100 times the initial boundary-layer thickness in both cases and the streamwise pressure gradient was nominally zero. Even such mild curvature, typical of aerofoils rather than turbomachine blades, can produce changes of the order of 10% in skin-friction coefficient. The main conclusion of the above studies was that the responses of a two-dimensional boundary layer to convex and concave curvatures were different, even qualitatively. Concave curvature increases turbulent mixing and gives rise to Taylor–Görtler roll cells, and convex curvature suppresses turbulent activity. There

† Over 'infinite' swept wings, the generators and the isobars are all parallel: gradients along the generators are zero, which simplifies analysis, but the turbulence structure is still representative of general three-dimensional boundary layers.

are also several other investigations into the effects of curvature on two-dimensional boundary layers with radius of curvature of about 10 times the initial boundary-layer thickness (strong curvature), such as those reported by Gillis & Johnston (1983) on convex curvature and Barlow & Johnston (1988) on concave curvature. Strong curvature causes very large changes in turbulence structure, even in the inner part of the boundary layer. In the present case, curvature effects are expected to be most important in the outer layer where the eddies are larger, and we have not attempted to explore the near-wall region in detail: a study of the near-wall region of a plane three-dimensional boundary layer using subminiature probes is long overdue.

It was realized at the so-called Trondheim trials (see East 1975) that turbulence models for two-dimensional flows, when extended to three-dimensional boundary layers by plausible arguments based on the rotation of coordinates, may not reproduce experimental results. For instance, the *isotropic eddy viscosity* hypothesis does not predict the observed fact that the shear stress and mean velocity gradient vectors have different directions. The magnitude of the shear stress in the outer layer ($y/\delta > 0.2$) is also overpredicted by using the typical value for two-dimensional boundary layers ($0.0168 U_e \delta^*$). It is by no means certain that the empirical formulae used to represent curvature effects in two-dimensional calculation methods would be applicable to three-dimensional shear flows. It is also not certain that the combined effects of mean flow three-dimensionality and longitudinal curvature are simply a superposition of the individual effects, since the response of a turbulent boundary layer to a given perturbation is often non-linear (Smits & Wood 1985). However, superposition implies a weak net effect of crossflow and concave curvature, while combined crossflow and convex curvature is expected to produce a large and significant decrease in the turbulence intensity. On the other hand, the totally different nature of the responses to concave and convex curvature found in the two-dimensional cases, suggests that the interaction in three-dimensional boundary layers may depend, even qualitatively, on the sign of curvature (i.e. concave or convex). In that case, the response of a three-dimensional boundary layer may be totally different for concave or for convex curvature. Therefore, the net effect of combined crossflow and streamline curvature on the behaviour of a turbulent boundary layer is an open question and there is a need for investigation. Hence, the next logical step in the sequence of the above studies at Imperial College was to extend the three-dimensional shear-layer work to include curvature. Simulation of such a flow also contains features of a more general configuration such as a transonic aircraft wing, where the upper surface is convex and the rear lower surface is generally concave. The present study is intended partly to serve as a test case for prediction methods for general three-dimensional shear layers and partly to improve our physical understanding of curvature effects in three-dimensional boundary layers.

The results of the present investigation show that the net effect of curvature and mean flow three-dimensionality on the turbulence structure is small, for mild curvature of either sign. In the case of concave curvature, the weak net effect is consistent with the opposing nature of the individual extra strain rates and qualitatively implies superposition. An unexpected finding (Baskaran & Bradshaw 1988) was that the spanwise wavy inhomogeneities ('Taylor–Görtler' vortices or roll cells – see Tani 1962 and Barlow & Johnston 1988) that occur in the two-dimensional flow decayed as the crossflow increased in the three-dimensional case. The only forewarning of the decay came from the calculations of Hall (1984), which showed that in laminar three-dimensional boundary layers the inflectional crossflow

instability, whose eigenmode is an array of co-rotating longitudinal vortices, overwhelms the contra-rotating longitudinal vortices of Taylor–Görtler instability. However, Bradshaw & Pontikos found no evidence for the crossflow instability modes in their three-dimensional turbulent boundary layer. Certainly, the decay of the spanwise variations in the concave case simplifies interpretation. The combined effect of crossflow and convex curvature is also small, though the two effects individually reduce the turbulence intensity and might have been expected to produce a large reduction in combination. In this case, the nonlinearity is obviously very strong.

Calculations by the method of Bradshaw, Mizner & Unsworth (1976) for three-dimensional boundary layers were done for all three cases (plane, concave and convex). This is an extension of the method for two-dimensional shear layers developed by Bradshaw, Ferriss & Atwell (1967), using partial-differential 'transport' equations for $-\overline{uv}$ and $-\overline{vw}$ and avoiding eddy viscosity altogether. It is used here as a subject for criticism merely because it is a simple, easily-available stress-transport model: more modern models would probably behave similarly. It can accommodate empirical corrections for curvature and other extra strain rates, which give good predictions of the effects of streamline curvature in two-dimensional boundary layers. Bradshaw (1971) demonstrated the capabilities and limitations of this method for three-dimensional boundary layers using the then available experiments for 'infinite' swept flows. The method predicts a skin friction distribution in fair agreement with the measurements in the concave case, but gives a poor prediction in the convex case. Since the method gives poor results for the plane case, owing to its failure to crossflow effects on the structure, the good agreement in concave case is a coincidence. Nevertheless, the pattern of discrepancies is consistent with the qualitative deduction from the experimental results, that the effects of crossflow and of concave curvature can be roughly superposed, but that there is a strong interaction between crossflow and convex curvature.

2. Apparatus and techniques

The experimental rigs, shown in figure 1, were generally similar to the ducted configuration used by Bradshaw & Pontikos, but with curved floors on which the boundary layers were studied. The rigs were attached to the exit of the blower tunnel used in the previous study. In each case, the duct consisted of a flat initial section of dimensions 762 mm × 127 mm, followed by a 35° swept section with a curved floor, together with an adjustable roof and curved sidewalls. The initial laminar boundary layer was removed by means of a 6 mm suction slot attached to an independent blower. The slot was swept at 35° to form the equivalent of the leading edge of a swept wing. A 50 mm wide swept sandpaper trip located immediately after the slot was used to promote transition and thicken the boundary layer. At the end of the front flat section the thickness of the turbulent boundary layer was 20 mm, with a momentum thickness Reynolds number of about 4000, in both cases. The radius of curvature of the swept curved floor was 2540 mm, giving about the same ratio of initial boundary-layer thickness to surface radius of curvature as that used in the earlier two-dimensional studies on mild streamline curvature at Imperial College (this ratio will be referred to as the 'curvature parameter' hereafter). At the start of curvature, the curvature parameter is 0.008. Note that the 'wall curvature perturbation parameter', $\nu\Delta k/U_{\tau 0}$, is only 0.04×10^{-4} (Δk is the step change in surface curvature, ν is the kinematic viscosity and $U_{\tau 0}$ is the friction velocity at the start of

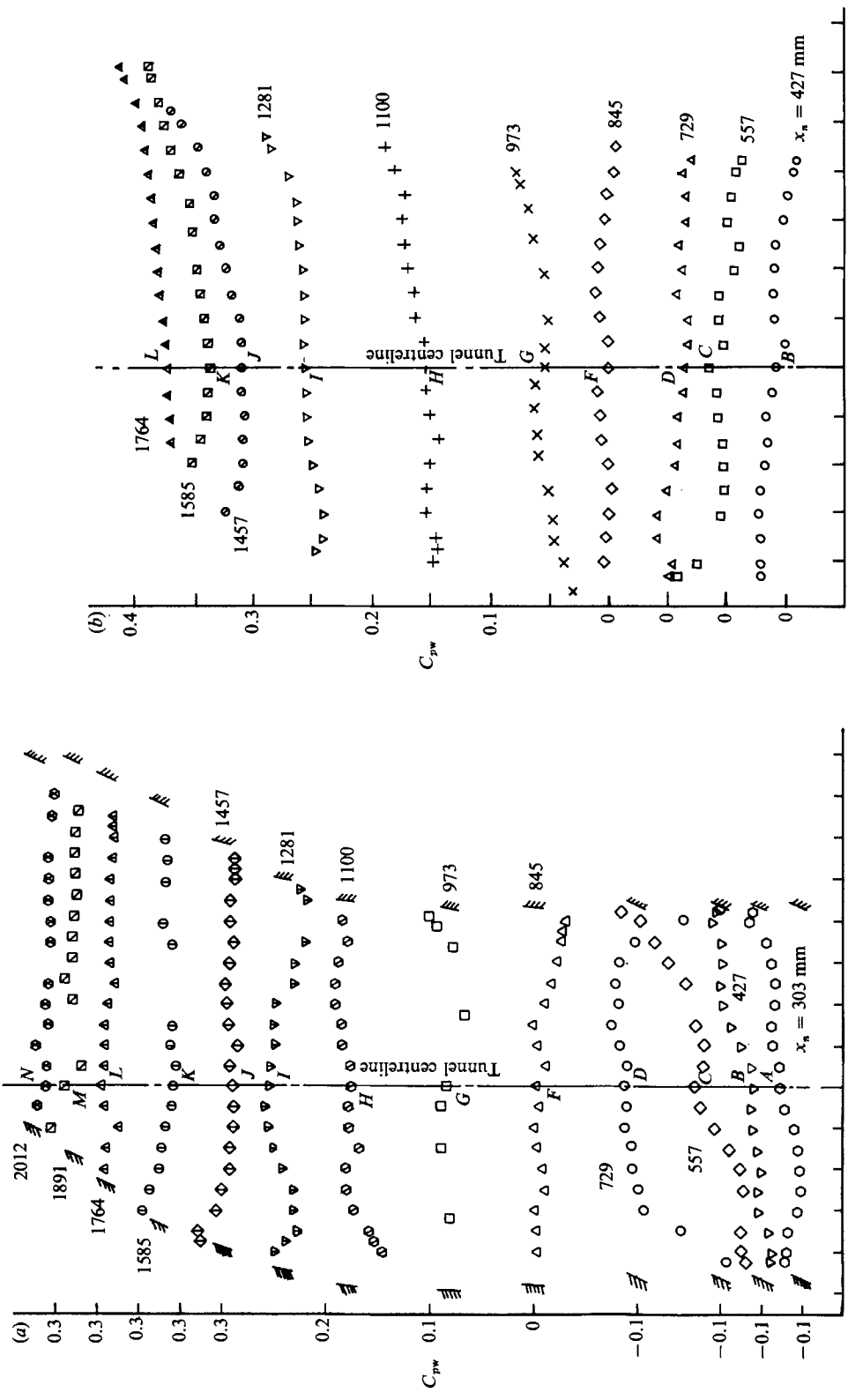

FIGURE 2. Surface pressure distribution along the generators (note shift in ordinate scale). (*a*) Concave curvature. (*b*) Convex curvature.

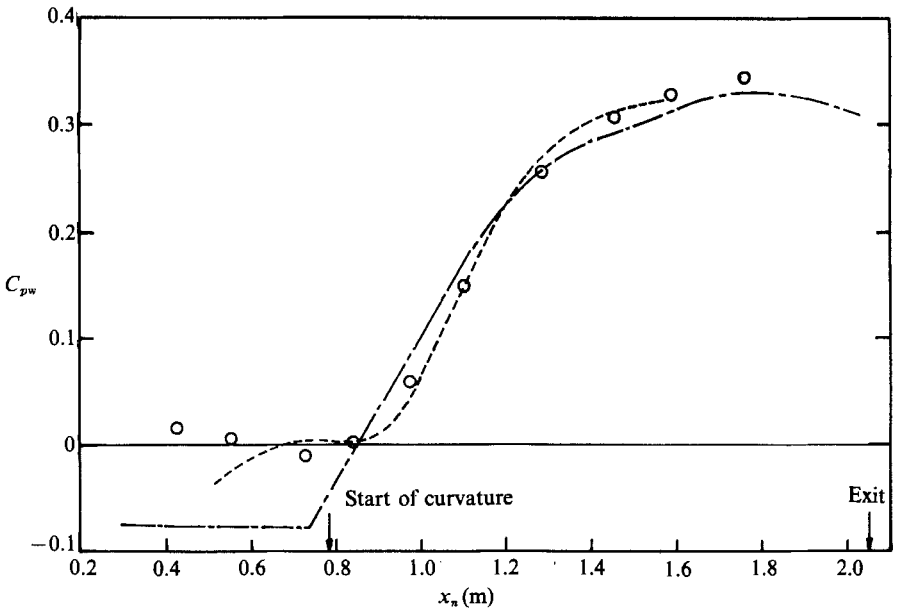

FIGURE 3. Surface pressure distribution normal to the generators. ----, flat wing of Bradshaw & Pontikos (1985); – – –, concave curvature; ○, convex curvature.

curvature), and the above definition of curvature parameter is still a meaningful representation of curvature effects, in contrast to strongly curved cases where the growth of an internal boundary layer confuses the effects of curvature (Baskaran, Smits & Joubert 1987). The curved sidewalls were adjusted by trial and error to simulate 'infinite' swept flow, and the static pressure distributions along the generators (referred to as the 'spanwise' direction) are shown in figure 2 (*a*, *b*) for the concave and convex curvature rigs respectively. Detailed measurements of skin-friction coefficient as a function of x and z in the concave case are given by Baskaran & Bradshaw (1988) and show that crossflow from the wall on the negative-z side does not reach the region where the main measurements were made. The flexible roofs of the curved sections were adjusted so that the surface pressure distributions normal to the generators (referred to as 'chordwise') approximated that in the 'infinite' swept flat-wing experiments, as shown in figure 3. At the last measurement station the upper and lower wall boundary layers were separated by about 110 mm of potential flow – roughly 1.5 to 2 times the test-wall boundary-layer thickness. The pressure gradient nominally starts at the same chordwise station as the curvature. The chordwise distributions of static pressure (and other quantities where shown) are matched with respect to the reference static pressure location. The external flow angle with respect to the tunnel axis (the x-axis in figure 1) at the boundary-layer edge is shown in figure 4 for the flat surface and curved flow cases. All measurements in the present study were conducted at a nominal tunnel free-stream velocity of 33 m/s, corresponding to a Reynolds number U_{ref}/ν of 2.2×10^6 per metre. The duct rig simulated a wing with a chord of 2 m, at a tiny fraction of the cost of testing a real wing in a large tunnel: the disadvantage is that, because of the method of construction, flow visualization is virtually impossible.

Some of the measurement procedures were slightly different in the two cases. In the concave case, the direction of the surface shear stress vector was measured using

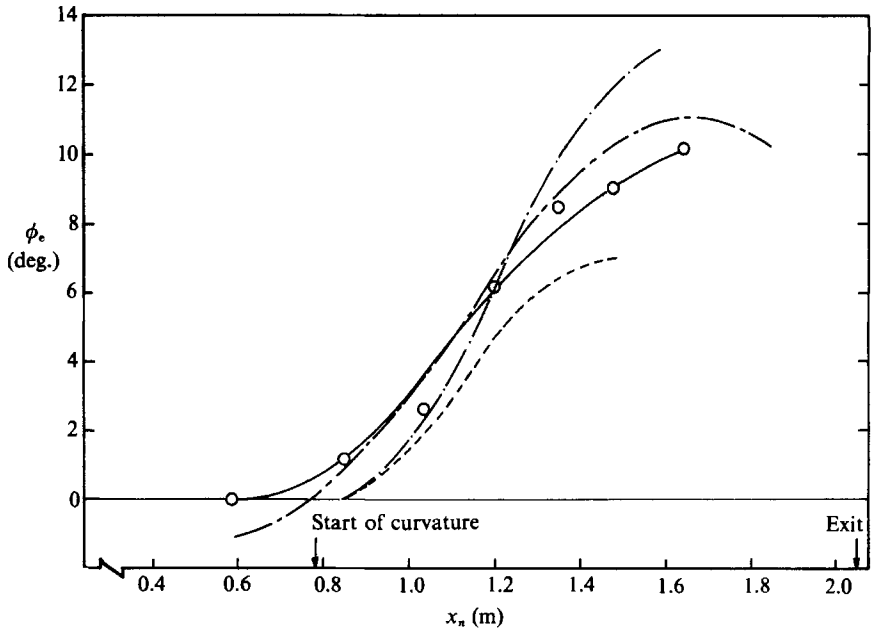

FIGURE 4. Direction of the edge streamline with respect to tunnel axis. ----, Bradshaw & Pontikos (1985); –·–, NLR data; – – –, concave curvature; –O–, convex curvature.

a 0.7 mm diameter three-hole surface yawmeter in non-null mode. The surface yawmeter was calibrated for yaw angle in the two-dimensional laminar boundary layer ahead of the suction slot. The magnitude of the surface shear stress was measured with a 1.1 mm diameter Preston tube aligned to the direction of surface shear stress using the calibration of Patel (1965). This assumes that the law of the wall is the same as in two-dimensional flow: for a discussion see §3.1. A three-hole probe of 0.89 mm diameter was used for mean velocity vector measurements in the boundary layer in non-null mode. This probe was calibrated for yaw angle, static pressure and total pressure in the undisturbed tunnel free stream using a procedure recommended by Bryer & Pankhurst (1971). In the convex case, the magnitude of the surface shear stress was measured with a Preston tube of 1.1 mm diameter, and a 0.89 mm three-hole probe, both aligned with the surface-flow direction. The same three-hole probe was nulled in the boundary layer for resultant mean velocity measurements, so that the surface flow direction could be obtained by extrapolation of the crossflow-angle profiles. In both cases, the static pressure distribution across the boundary layer was measured with the three-hole probe.

Turbulence measurements were made using crossed hot-wire probes. The probes were home-made with platinum core Wollaston wire of 5 μm diameter, soft soldered to the prongs and etched to give an active length of about 1.2 mm. (This implies poor spatial resolution at wall distances less than about 3 mm, and we did not make turbulence measurements in this region.) Melbourne University type constant temperature anemometers were used, with a prefixed resistance ratio of 1.8. The wires were statically calibrated before every profile. The effective wire angles were determined through a yaw calibration (Bradshaw 1971), giving the best fit to the cosine cooling law. All measurements were conducted with the axis of the probe parallel to the tunnel axis, as in the earlier 'infinite' swept flat wing experiments. The

measurements included all six components of the Reynolds stress tensor, and all the triple products that appear in the transport equations for the Reynolds stress components. Some selected fourth-order quantitites were also obtained. The correlations between v and w fluctuations were obtained by rolling the probe about its axis into $\pm 45°$ planes, so that the wires responded to $(v \pm w)/\sqrt{2}$. The cross-stream shear stress, $-\overline{vw}$, and the associated triple products, viz. $\overline{v^2w}$, $\overline{vw^2}$ and $\overline{vvw}$, were deduced as the sums and differences of the quantities corresponding to these two planes, as explained by Baskaran & Bradshaw (1987). All turbulence measurements in the concave case were obtained on-line using a sample/hold unit, a Tecmar/Labmaster 12 bit analog-to-digital converter and an IBM-PC 'portable' micro-computer programmed in Microsoft Fortran. Twenty thousand samples per wire per roll plane were collected at each point in the boundary layer at a sampling frequency of 200 Hz. In the convex rig experiments, the hot-wire signals from the four roll planes were recorded on analog tape using an SEL 3000 tape recorder and later digitized for batch processing on the College Cyber computers, including the linearizations of hot-wire calibrations. The absolute accuracy of hot-wire measurements is always difficult to assess: the probes and techniques used in the two experiments described here (and in the measurement of Bradshaw & Pontikos) were very similar, and comparisons between the different flows therefore depend only on repeatability. Repeatability checks for the hot-wire data are given in detail in Baskaran & Bradshaw (1987). At the last measurement station near the peak normal stress location, where the crossflow with respect to the hot-wire probe is the largest, the normal stress components were repeatable to 5%, the shear stress component, $-\overline{uv}$, to 15% and the shear stress components, $-\overline{vw}$ and $-\overline{uw}$, to 30%.

3. Results

3.1. *Concave curvature*

The chordwise distributions of the skin friction coefficient, C_f $(= 2(Q_\tau/Q_e)^2)$ and the relative surface crossflow angle, $\beta_w (= \phi_w - \phi_e)$ for the 'infinite' swept three-dimensional boundary layer with concave curvature are shown in figure 5. The decrease in the earlier part of the flow is principally due to the adverse pressure gradient: the boundary-layer thickness δ increases by a factor of about 4 over the length of the flow, so that two-dimensional flat-plate skin friction would decrease by about 25%. In the above relations, Q_τ and ϕ_w are the magnitude and direction of the friction velocity along the wall streamline and the suffix 'e' refers to the edge streamline just outside the boundary layer. In two-dimensional curved-wall boundary layers, it is common to use the potential wall velocity, $U_{pw} (= U_{ref}(-C_{pw})^{\frac{1}{2}}$, instead of the edge velocity, whose magnitude in the present case is not much different, as we shall see later. Also shown in the same figure are the distributions predicted by the method of Bradshaw *et al.* (1976) with and without an empirical curvature correction (based on two-dimensional data): the performance of the method in the different cases will be discussed below. The spanwise skin-friction distributions over the 'infinite' swept concave wing, discussed in Baskaran & Bradshaw (1988), show clearly the decay of wavy inhomogenities that normally exist in two-dimensional concave wall boundary layers owing to Taylor–Görtler roll cells.

The static pressure distributions across the boundary layer are shown in figure 6. (The pressure-coefficient difference across a boundary layer with $\delta/R \approx 0.01$ is expected to be less than 0.02.) The surface pressure coefficients, inferred from figure 3 for the different chordwise stations, are also plotted in figure 6: the distributions

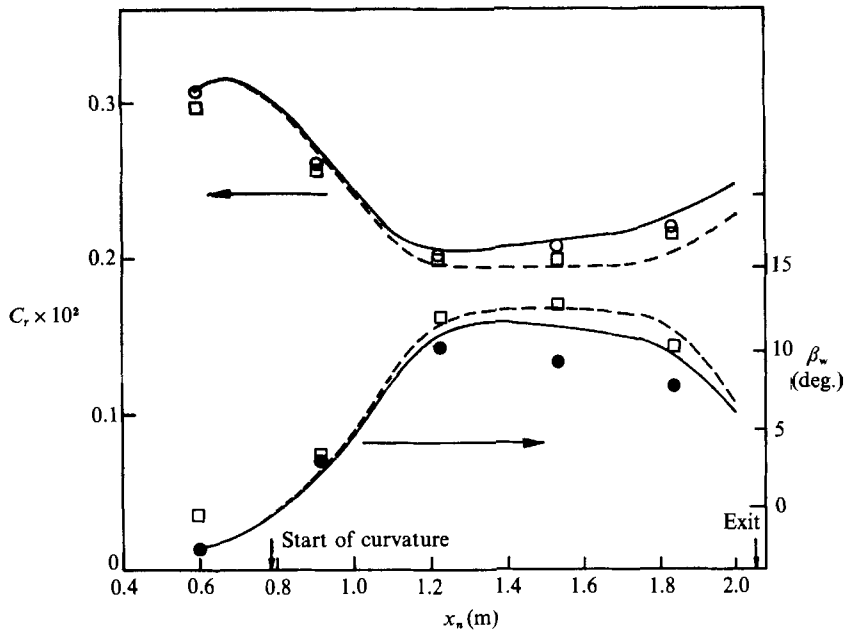

FIGURE 5. Chordwise skin friction and crossflow distributions over the concave wing. ○, aligned Preston tube (1.1 mm dia); □, law of the wall; ●, 3-hole surface yawmeter (0.7 mm dia.); calculation of Bradshaw, Mizner & Unsworth (1976): —, with curvature correction; ---, without curvature correction.

close to the surface (about the first 7 data points) are obviously inaccurate, owing to wall proximity effects on the response of the three-hold probe, and should not be taken seriously. If these points are ignored, the static pressure distributions in the boundary layer extrapolate fairly well to the values at the surface, giving confidence in the yawmeter measurements (which are well-conditioned for flow angle and total pressure but yield the static pressure as the small difference of two large quantities). The magnitude of the resultant mean velocity vector, non-dimensionalized by the local potential velocity, Q_p, and its direction relative to the local edge streamline are shown in figure 7. The potential velocity was inferred using the total pressure outside the boundary layer and the local static pressure. The profiles of the resultant mean velocity magnitude are unremarkable. At the last station ($x_n = 1839$ mm), the pressure gradient tends to relax and the increase in the mean velocity gradient is consistent with the expected trend in the inner region. Again owing to the wall proximity effect on the three-hole probe, the flow angles near the wall are overestimated, apparently by as much as 2°, and this discrepancy also appears in the flow angle profiles of Bradshaw & Pontikos. The wall interference effect on the behaviour of three-hole yaw probes deserves scrutiny in both laminar and turbulent boundary layers, for both null and non-null applications†.

The mean flow profiles are plotted in the wall coordinate system for the resultant velocity in figure 8. In these plots, the conventional displacement correction was applied to the wall distance by adding 15% of the probe diameter. In three-

† Baskaran & Bradshaw (1987) present calibrations for the three-hole probe at different distances from the wall in a laminar boundary layer. The mean flow data presented here are based on the free-stream calibration so that the comparisons with the convex and flat surface cases are valid.

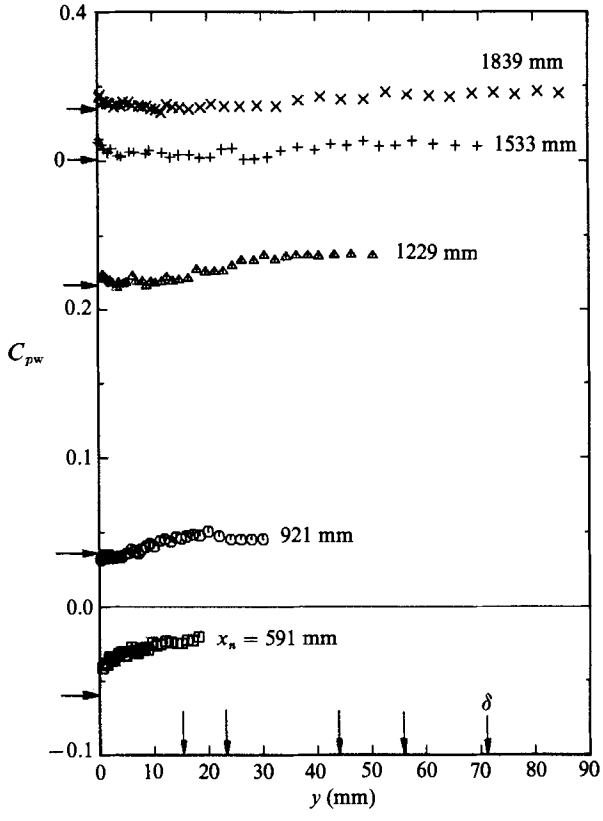

FIGURE 6. Static pressure distributions across the boundary layer over the concave wing. →, from figure 3.

dimensional turbulent boundary layers with mild crossflow, the validity of the two dimensional law of the wall for the velocity magnitude was verified by Pierce & Zimmerman (1973), and Fernholz & Vagt (1981). (Note that the pressure measured by a Preston tube is independent of yaw angle over a range of at least $\pm 10°$, so that, if aligned with the flow direction at or near the surface, the tube will respond to the velocity magnitude and therefore give acceptable answers as long as the law of the wall holds in the above sense.) Bradshaw & Pontikos found that the region of validity of the two-dimensional logarithmic law with constants 0.41 and 5.2 (de Brederode & Bradshaw 1974) decreased with an increase in the crossflow. In the concave case, the friction velocity was inferred by plotting the resultant mean velocity on a Clauser chart as in the flat-surface case. The points suspected to be affected by wall interference (based on figure 6) were discarded in the Clauser fits. The dip below the logarithmic law usually observed in two-dimensional concave wall boundary layers is absent. The outer limit of the logarithmic region increases slightly as the crossflow increases in the present concave case. Johnston (1970) also observed a similar increase in the outer limit for the logarithmic region in his three-dimensional boundary layer induced by a swept forward-facing step, where the streamline curvature was concave. The wake component initially increases owing to the adverse pressure gradient, before decreasing at the last station owing to a favourable pressure gradient, as expected. We have also inferred the direction of the friction velocity

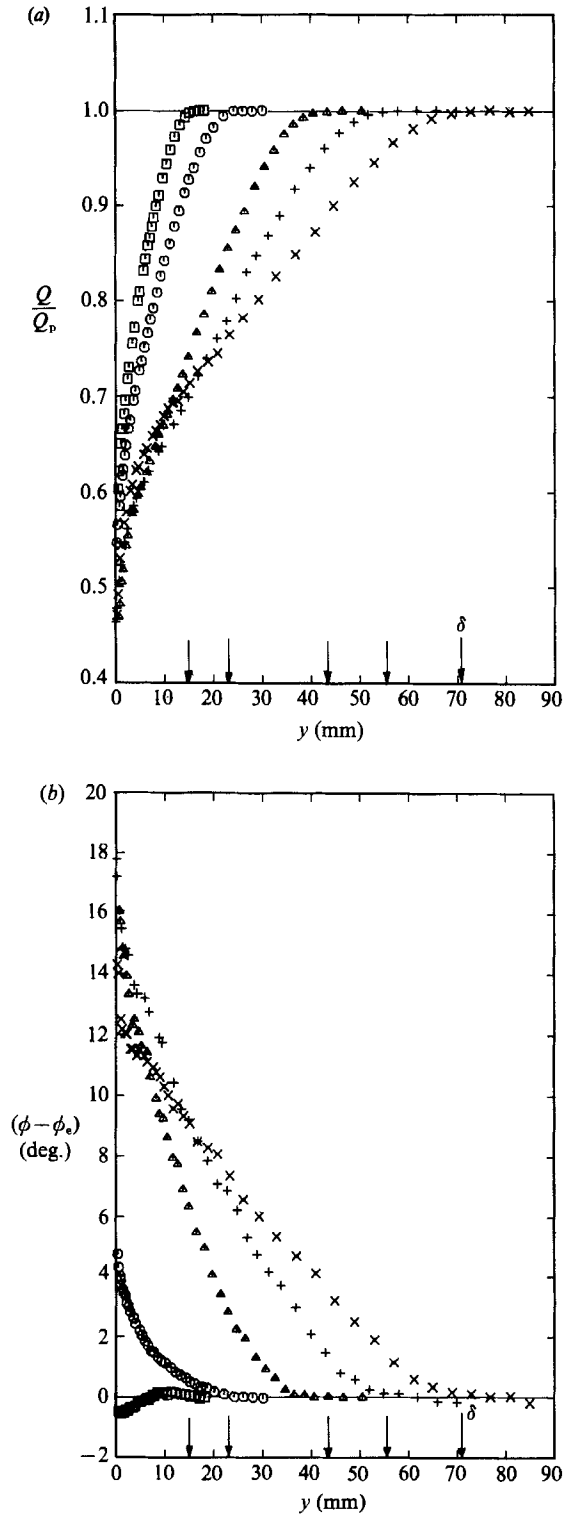

FIGURE 7. Resultant mean velocity profiles over the concave wing. (*a*) Magnitude. (*b*) Direction relative to the edge streamline.

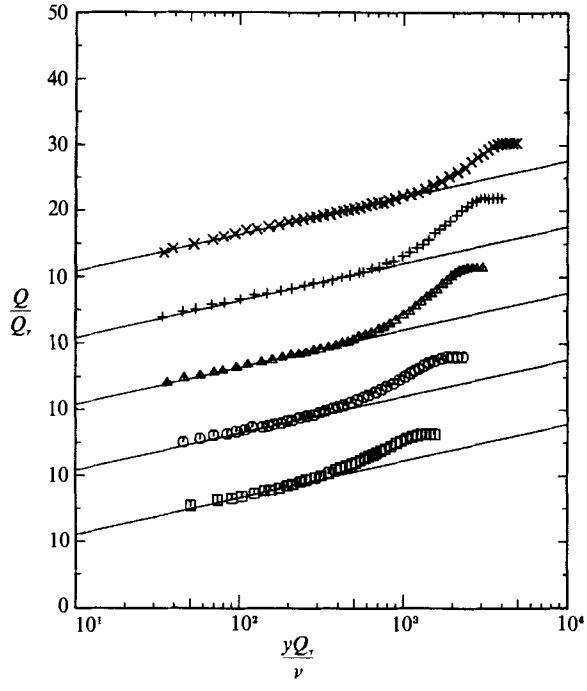

FIGURE 8. Resultant mean velocity profiles in wall coordinates for the concave wing.

x_n (mm)	δ^*_{11} (mm)	δ^*_{22} (mm)	θ_{11} (mm)	θ_{22} (mm)	H_{11}	H_{22}
591	2.62	−0.024	1.71	—	1.53	—
921	4.12	−0.391	2.767	−0.01	1.49	—
1229	8.58	−2.414	5.604	−0.228	1.53	10.61
1533	11.33	−4.124	7.46	−0.428	1.52	9.64
1839	12.96	−4.864	9.087	−0.456	1.43	10.67

TABLE 1. Integral parameters for the 'infinite' swept concave wing (evaluated in coordinates aligned to the edge streamline: negative values are a consequence of crossflow in the positive-z direction)

from the law of the wall using an iterative procedure, where the law of the wall was fitted to the velocity component in the directions of the tunnel axis and the wall streamline. Normally, large changes in the local flow direction in a three-dimensional turbulent boundary layer occur within the viscous sublayer, whose outer edge corresponds to the apex in the polar triangular plot for the mean flow. In the present case, however, the change in the flow direction is small between the inner (apex) and the outer limits of the logarithmic region (about 4° over the range of data points actually fitted) and the method is viable. The initial direction of the wall shear stress vector was taken as arcos (U_τ/Q_τ) where U_τ and Q_τ are the friction velocities obtained with the component of resultant velocity in the direction of the tunnel axis and the resultant velocity itself. Then the resultant mean velocity vector was resolved in the direction of the wall shear stress vector and the logarithmic law fitted. This gives the new value for the direction of the wall streamline. The procedure is repeated till

the successive iterations are within half a per cent. The distribution of the wall streamline direction is compared with the independent measurements in figure 5.

The relations for the integral parameters such as the displacement thickness, momentum thickness and the shape factor were adopted from Cooke & Hall (1962) with the constant potential velocity, U_e, replaced by the local potential velocity, Q_p. Integral parameters were evaluated in a coordinate system aligned with the edge streamline and are given in table 1 for the concave wing. The shape parameter, H_{11}, in the stream direction exhibits little change and is closely the same as that reported by Bradshaw & Pontilos on a flat surface. Both adverse pressure gradient and destabilizing curvature, individually tend to increase the shape factor in two-dimensional flows. However, the favourable pressure gradient at the end of the rig causes the shape factor to decrease. The other shape factor, H_{22}, remains approximately constant at the last three stations as the surface crossflow angle relative to the local external stream, β_w, itself remains nearly constant.

The six components of the Reynolds stress tensor for the chordwise stations are shown in figure 9. All these stresses are referred to the coordinates aligned to the tunnel axis, so that the changes can be considered as a spanwise perturbation of an initially two-dimensional flow. The components are non-dimensionalized with respect to the reference velocity, U_{ref}, in order to identify the absolute changes. The normal stress profiles are qualitatively similar to those reported by Bradshaw & Pontikos: the profiles contain a peak which moves away from the wall as the crossflow increases, and their changes are unremarkable. The shear stress component $-\overline{uv}$ decreases only slightly relative to the undisturbed flow, unlike the huge decrease (about 50% in the maximum value) reported by Bradshaw & Pontikos for the same crossflow range. The $-\overline{vw}$ profiles behave differently, in that the multiple peaks reported by Bradshaw & Pontikos are absent, and our profiles of $-\overline{uw}$ change sign relatively closer to the wall. The profiles of $-\overline{vw}$ at the last two stations are not wholly reliable, as indicated by the disagreement between the independently measured wall values and the first $-\overline{vw}$ data point. This is presumably due to the crossflow relative to the probe being large, even though this does not seem to affect the $-\overline{uv}$ profiles: the distributions near the wall tend to extrapolate to the wall values fairly well, and the shear stress gradient is consistent with the pressure gradient close to the wall. Because the crossflow in all the experiments was roughly the same, the errors due to misalignment of the crosswire probe (aligned to x-axis) with respect to the local flow should not in principle jeopardize comparisons between the flat, concave and convex cases.

3.2. *Convex curvature*

The chordwise distributions of the skin friction coefficient and the relative surface crossflow angle for the convex case are shown in figure 10. Calculations by the method of Bradshaw *et al.* (1976) with and without the two-dimensional curvature correction are shown on the same figure. Unlike the concave case, the calculations do not agree well with the data.

The static pressure distributions across the boundary layer, shown in figure 11, once again extrapolate reasonably well to the surface values. The profiles of the resultant mean velocity vector are shown in figure 12, and the increase in the mean velocity gradient is consistent with the decreasing pressure gradient at the last station. The profile at the last station also exhibits a pronounced inflection typical of a two-dimensional mean flow profile approaching separation, even though 'separation', in three-dimensional boundary layers, does not require the resultant

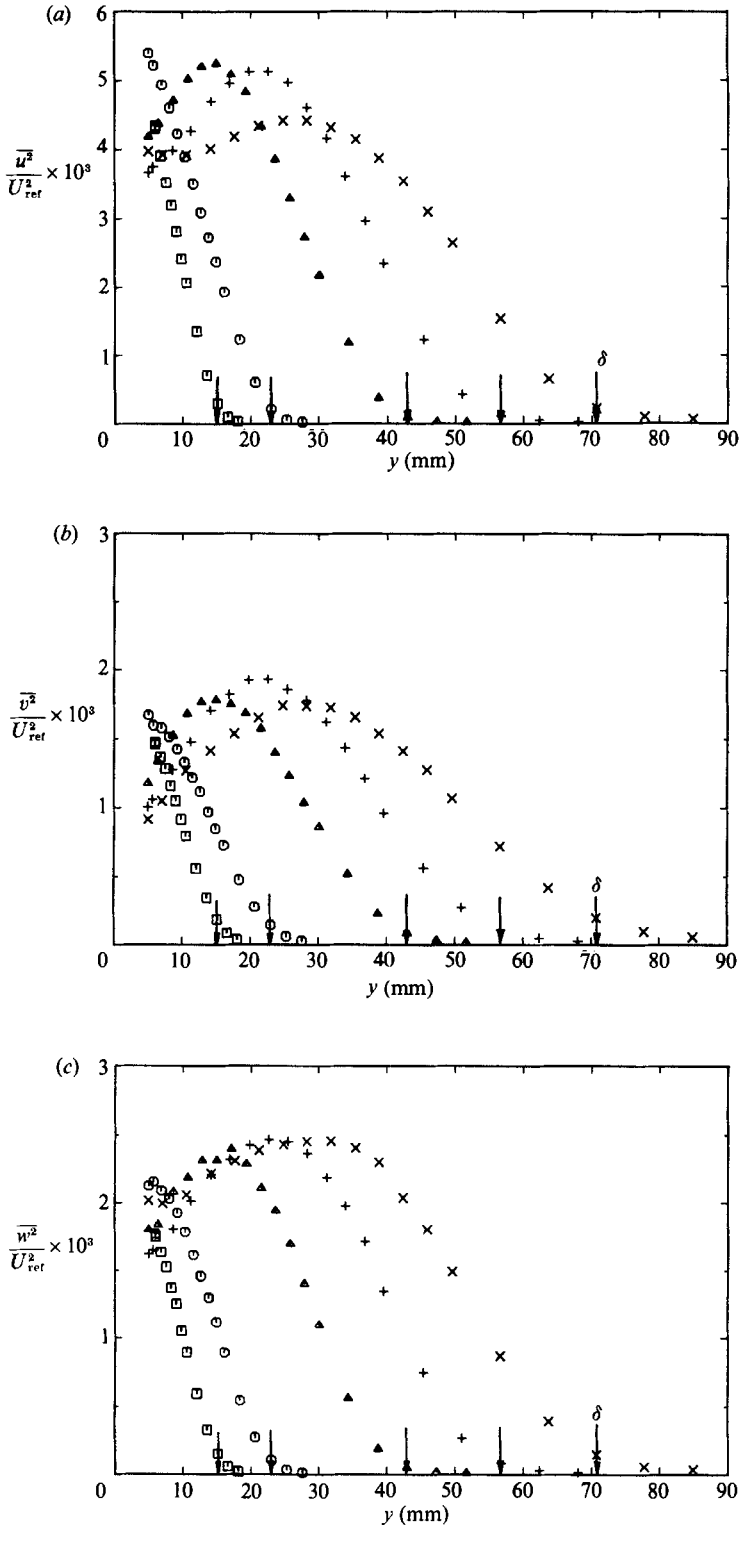

FIGURE 9(*a–c*). For caption see facing page.

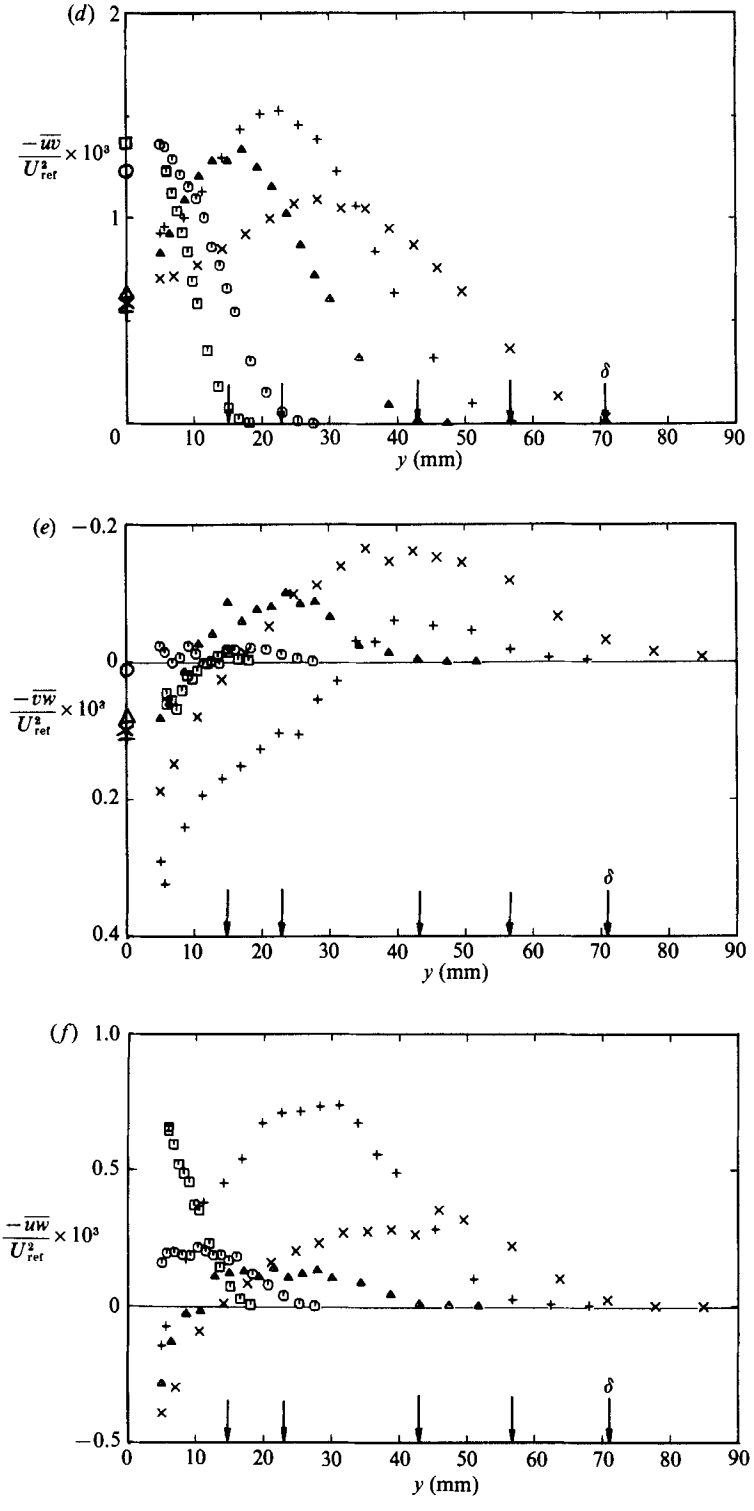

FIGURE 9. Profiles of Reynolds stress components for the concave wing. (*a*) $\overline{u^2}/U_{ref}^2$; (*b*) $\overline{u^2}/U_{ref}^2$; (*c*) $\overline{w^2}/U_{ref}^2$; (*d*) $-\overline{uv}/U_{ref}^2$; (*e*) $-\overline{vw}/U_{ref}^2$; (*f*) $-\overline{uw}/U_{ref}^2$.

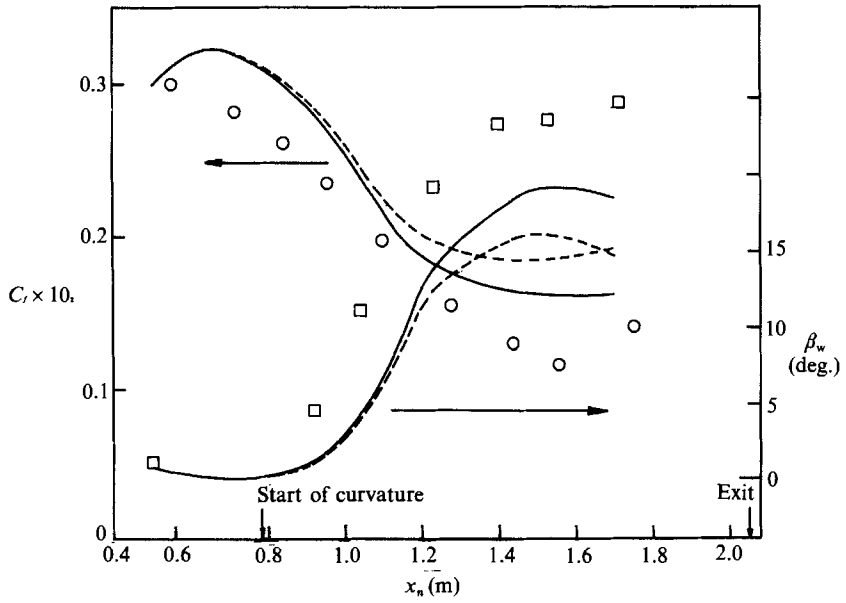

FIGURE 10. Chordwise skin friction and crossflow distibutions over the convex wing. ○, aligned Preston tube (1.1 mm dia); □, nulled 3-hole yawmeter (0.89 mm dia.); calculation of Bradshaw *et al.* (1976): —, with curvature correction; ---, without curvature correction.

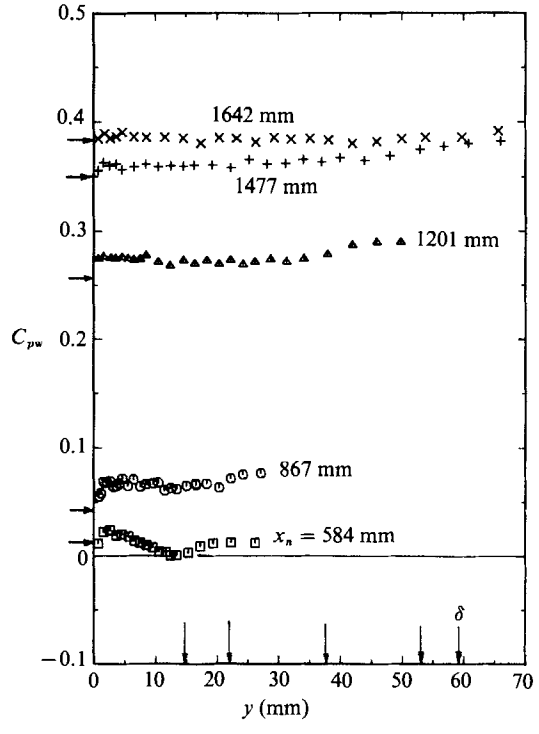

FIGURE 11. Static pressure distribution across the boundary layer over the convex wing. →, from figure 3.

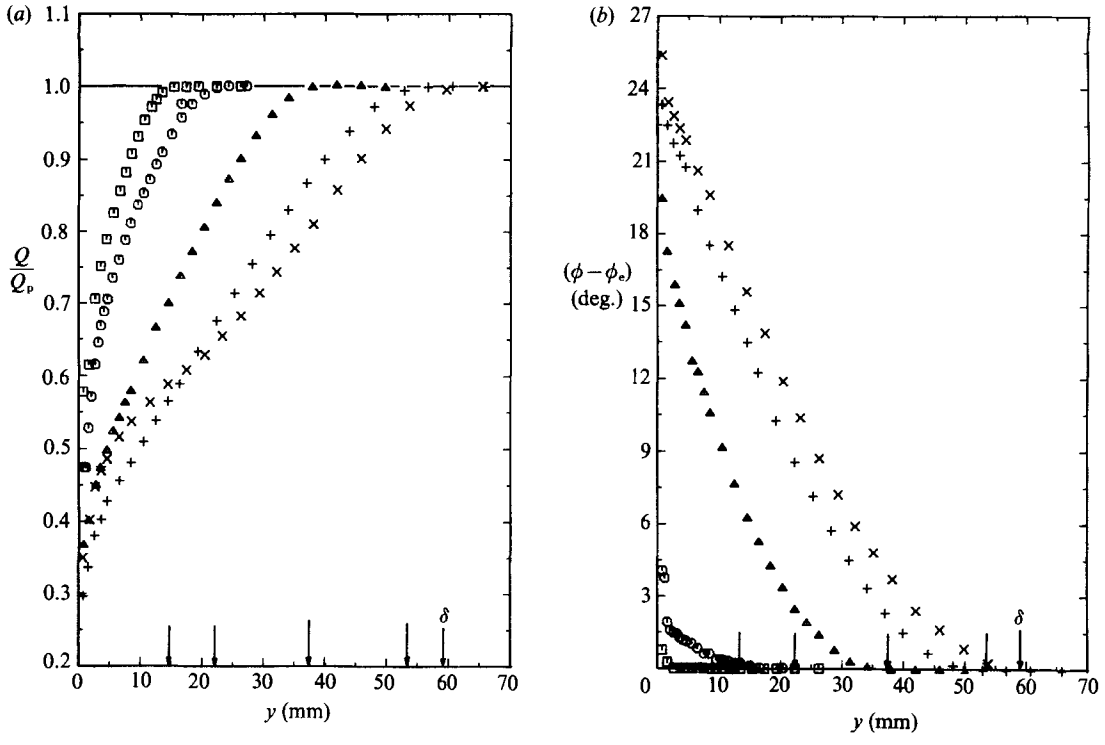

FIGURE 12. Resultant mean velocity profiles over the convex wing. (*a*) Magnitude. (*b*) Direction relative to the edge streamline.

x_n (mm)	δ^*_{11} (mm)	δ^*_{22} (mm)	θ_{11} (mm)	θ_{22} (mm)	H_{11}	H_{22}
584	2.48	−0.008	1.59	—	1.56	—
867	3.99	0.163	2.55	−0.003	1.57	—
1201	9.61	−2.16	5.6	−0.198	1.72	10.93
1477	15.71	−4.13	8.65	−0.473	1.82	8.74
1642	16.94	−5.34	9.96	−0.72	1.7	7.42

TABLE 2. Integral parameters for the 'infinite' swept convex wing (evaluated in coordinates aligned to the edge streamline).

shear stress to fall to zero. The flow angles close to the wall are suspected to be overestimates, owing to wall interference effects on the three-hole probe. The values at the wall were not measured independently and the 'surface' crossflow data in figure 10 are actually the first data points from the respective profiles shown in figure 12 (*b*). The integral parameters for the convex case are given in table 2. The increase in the shape factor H_{11} indicates that the mean flow profiles are considerably distorted and H_{22} gradually decreases as the relative surface crossflow increases.

The non-dimensionalized Reynolds stress components are shown in figure 13 for the convex case at different chordwise stations. As in the other cases, the profiles develop peaks and the distance of the peak from the wall increases as the flow moves downstream. $\overline{u^2}$ behaves qualitatively similarly, while both $\overline{v^2}$ and $\overline{w^2}$ show considerable differences between the wall and the location of maxima. The shear

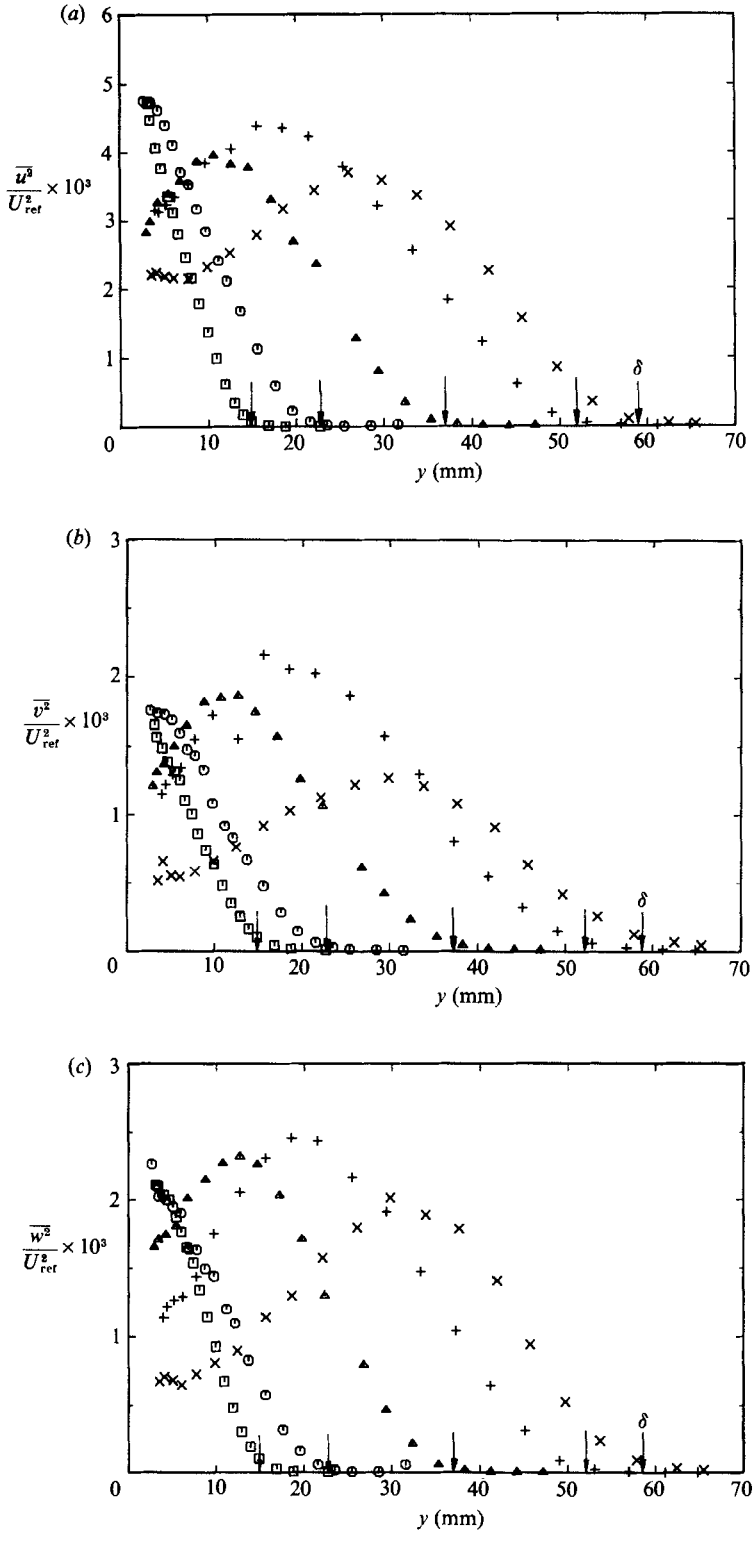

FIGURE 13(a–c). For caption see facing page.

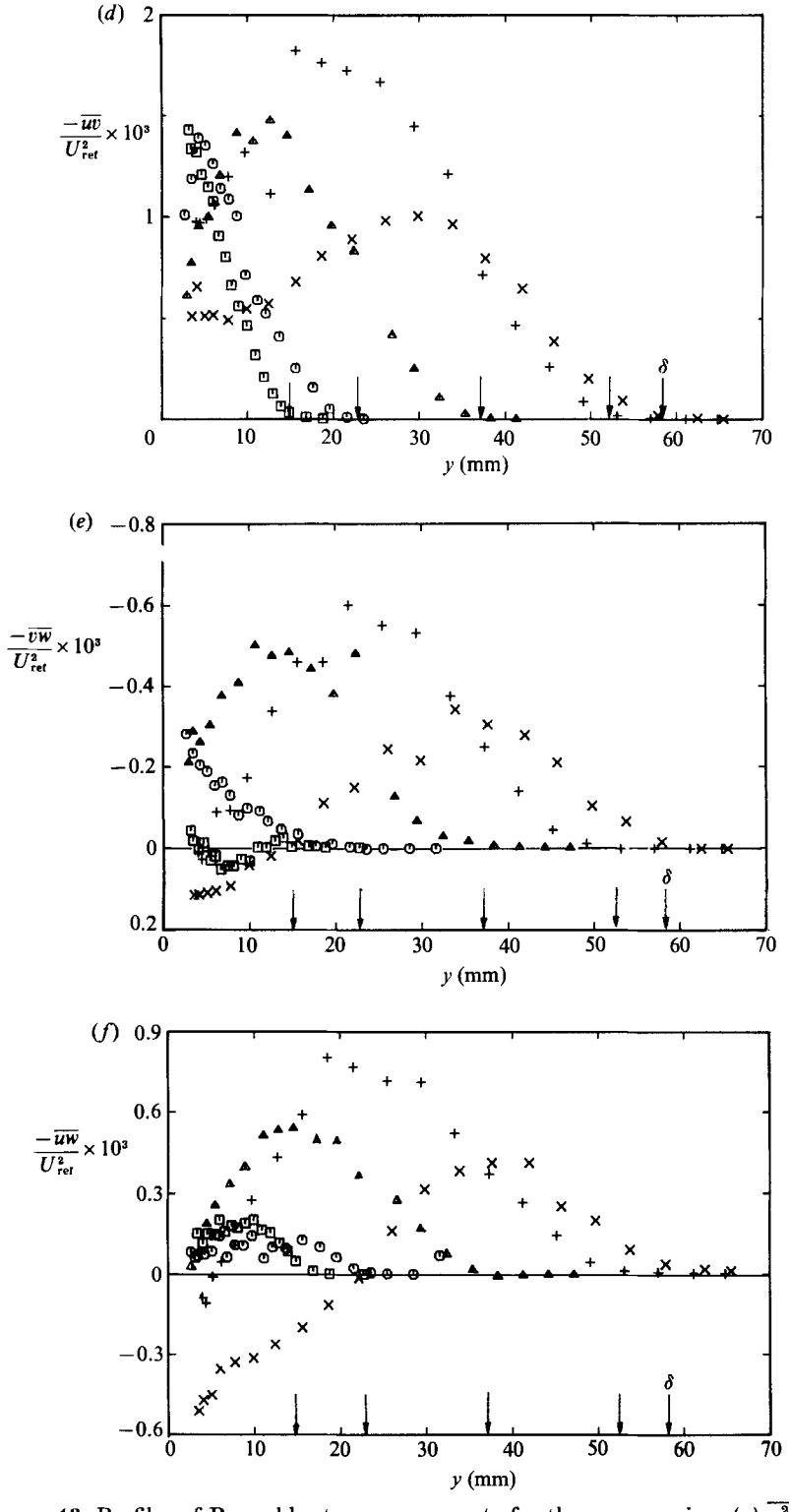

FIGURE 13. Profiles of Reynolds stress components for the convex wing. (*a*) $\overline{u^2}/U_{ref}^2$; (*b*) $\overline{u^2}/U_{ref}^2$; (*c*) $\overline{w^2}/U_{ref}^2$; (*d*) $-\overline{uv}/U_{ref}^2$; (*e*) $-\overline{vw}/U_{ref}^2$; (*f*) $-\overline{uw}/U_{ref}^2$.

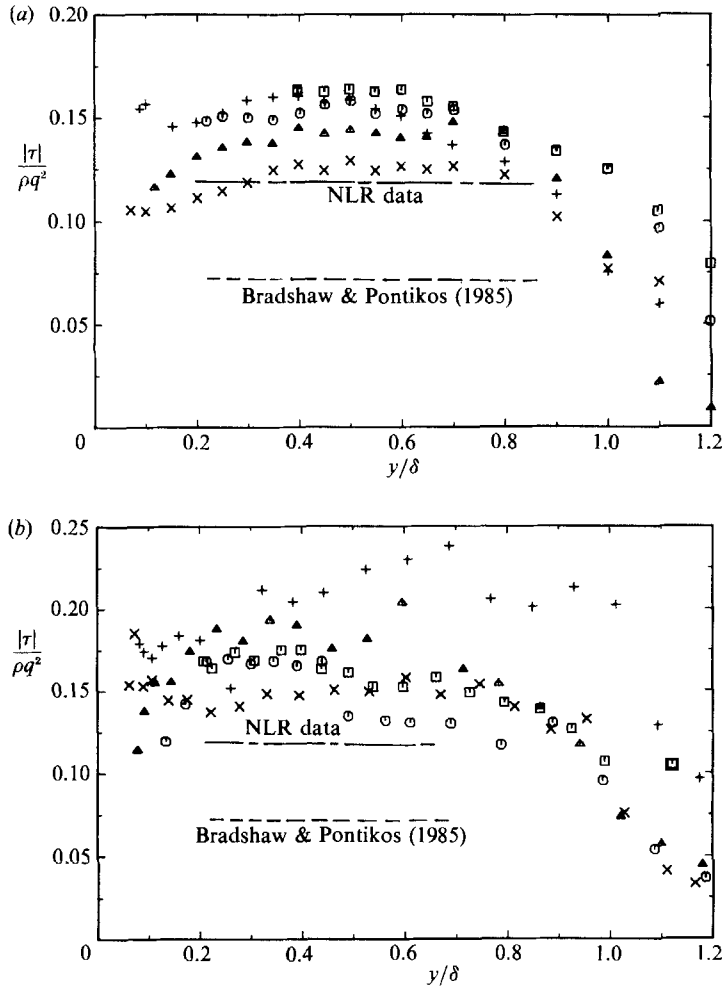

FIGURE 14. Ratio of the resultant shear stress to twice the total turbulent kinetic energy. (*a*) Concave curvature. (*b*) Convex curvature.

stress component $-\overline{uv}$ shows qualitatively much the same trend with downstream distance as in the profiles over the concave wing. This is unexpected, because in two-dimensional flows, $-\overline{uv}$ is very sensitive to the sign of curvature. The profiles of $-\overline{vw}$ again behave qualitatively similarly, but remain largely negative over most of the boundary-layer thickness. The profiles of $-\overline{uw}$ are qualitatively similar to those corresponding to the flat surface and concave cases.

4. Discussion

4.1. *Interaction of crossflow and mild streamline curvature*

The distributions of the structure parameter, a_1, represented in three-dimensional turbulent boundary layers as the ratio of the resultant shear stress magnitude, $\tau \equiv ([(-\overline{uv})^2+(-\overline{vw})^2]^{\frac{1}{2}})$ to twice the turbulent kinetic energy, $\overline{q^2}(\equiv \overline{u^2}+\overline{v^2}+\overline{w^2})$, are shown in figure 14 for both concave and convex curvature. Both these quantities are independent of rotation about the y-axis. Like most turbulence structure parameters,

a_1 is not strongly affected by pressure gradient, so the small differences in pressure gradient between the two cases can be ignored in discussion. In both cases, the changes in a_1 with crossflow, say with β_w, are much smaller than the significant reduction of the structure parameter (0.07) over nearly the same range of crossflow in the flat surface case of Bradshaw & Pontikos. Note that the NLR experiments reported by van den Berg *et al.* and Elsenaar & Boelsma did not exhibit such a large reduction in a_1, even though the surface crossflow is three times that of Bradshaw & Pontikos. This appears to be due to the difference in the individual behaviour of both $-\overline{uv}$ and $\overline{q^2}$. In the flow of Bradshaw & Pontikos $-\overline{uv}$ decreased strongly, while $\overline{q^2}$ remained unchanged with an increase in the crossflow. In the NLR experiments, both $\overline{q^2}$ and $-\overline{uv}$ actually increased with crossflow from the values in the undisturbed flow: for the same range of crossflow ($\beta_w = 0° - 17°$), $\overline{q^2}/\overline{q_0^2} \approx 7$ and $-\overline{uv}/-\overline{uv}_0 \approx 6$, both at $y/\delta \approx 0.5$, where suffix '0' refers to the values in the undisturbed flow. The increase in $\overline{q^2}$ in the NLR flow is predominantly due to a large rise in $\overline{w^2}$. Anderson & Eaton (1987) also observed increases in both $\overline{q^2}$ and $-\overline{uv}$, including a large increase in $\overline{w^2}$, in their pressure driven three-dimensional boundary layers. The precise reason for the difference in the behaviour of turbulent kinetic energy and the streamwise component of the shear stress in the case of Bradshaw & Pontikos is not clear. Nevertheless, the structure parameter, a_1, which is dimensionless and hence a meaningful quantity to compare between different experiments, decreases in all the above mentioned flat-surface cases.

The smaller change of a_1 in the three-dimensional concave case is consistent with superposition, in that mean flow three-dimensionality reduces the structure parameter, while concave curvature in two-dimensional flows increases it. In the convex case, the superposition argument would predict large changes in a_1 since convex curvature in two-dimensional flow reduces it. The experimental results in the convex case contradict this argument and imply that there is a strong interaction between the effects of crossflow and of convex streamline curvature. (This suggests that the superposition argument may not be trustworthy in general, even in the case of concave curvature.) These differences in the interaction of the effects of curvature and mean-flow three-dimensionality are further demonstrated below, using other quantities such as the transport velocities of turbulent kinetic energy, V_q, and of the shear stress component, V_{uv}, both being known to be sensitive to curvature in two dimensions. The y-component transport velocities are defined, after neglecting the unmeasurable pressure fluctuations, as

$$V_q = \frac{\overline{u^2v} + \overline{v^3} + \overline{w^2v}}{\overline{q^2}}, \quad V_{uv} = \frac{\overline{uv^2}}{\overline{uv}}.$$

Profiles of V_q and V_{uv} are shown in figures 15 and 16 respectively, for the concave and convex cases. Profiles of the individual triple products in the above relations are given in Baskaran & Bradshaw (1987) for concave curvature and in Baskaran, Pontikis & Bradshaw (1987) for convex curvature. The changes in the inner part of the layer, including the negative values for the transport velocities, are consistent with the distributions usually seen in adverse pressure gradient (East, Sawyer & Nash 1979). The distributions of V_q and V_{uv} in the outer portions of the layer show little change in either case, demonstrating that transport of energy and stress are not altered by the combined action of crossflow and curvature, unlike the decrease found in the flat-surface case. Considering the enhancement by concave curvature, and the attenuation by convex curvature, of turbulent transport in two-dimensional

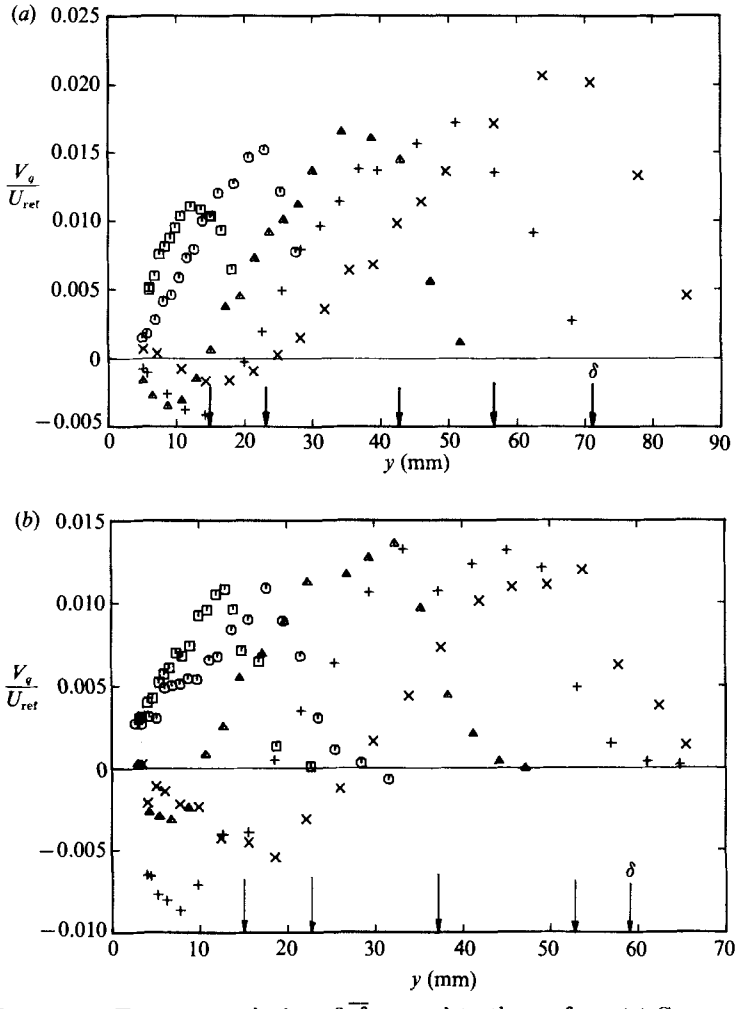

FIGURE 15. Transport velocity of $\overline{q^2}$ normal to the surface. (*a*) Concave curvature; (*b*) Convex curvature.

boundary layers, the small changes in the transport velocities in curved three-dimensional boundary layers support the apparent superposition of crossflow and curvature effects in the case of a concave wing and a nonlinear interaction between the two effects in the convex wing boundary layer.

4.2. *Implications for turbulence modelling*

In two-dimensional boundary layers, the directions of the shear stress vector and the mean velocity gradient vector are necessarily coincident. Turbulence models which extend the eddy viscosity hypothesis for two-dimensional flows to three-dimensional boundary layers usually assume that the eddy viscosity is isotropic, specifically that the components along and across the local mean flow are equal. The eddy viscosity components along and across the local mean flow, ν_{sm} and ν_{cm}, are defined respectively as,

$$\nu_{sm} = -\overline{u_m v}/|\partial Q/\partial y|\cos\phi_{gm},$$

$$\nu_{cm} = -\overline{v w_m}/|\partial Q/\partial y|\sin\phi_{gm},$$

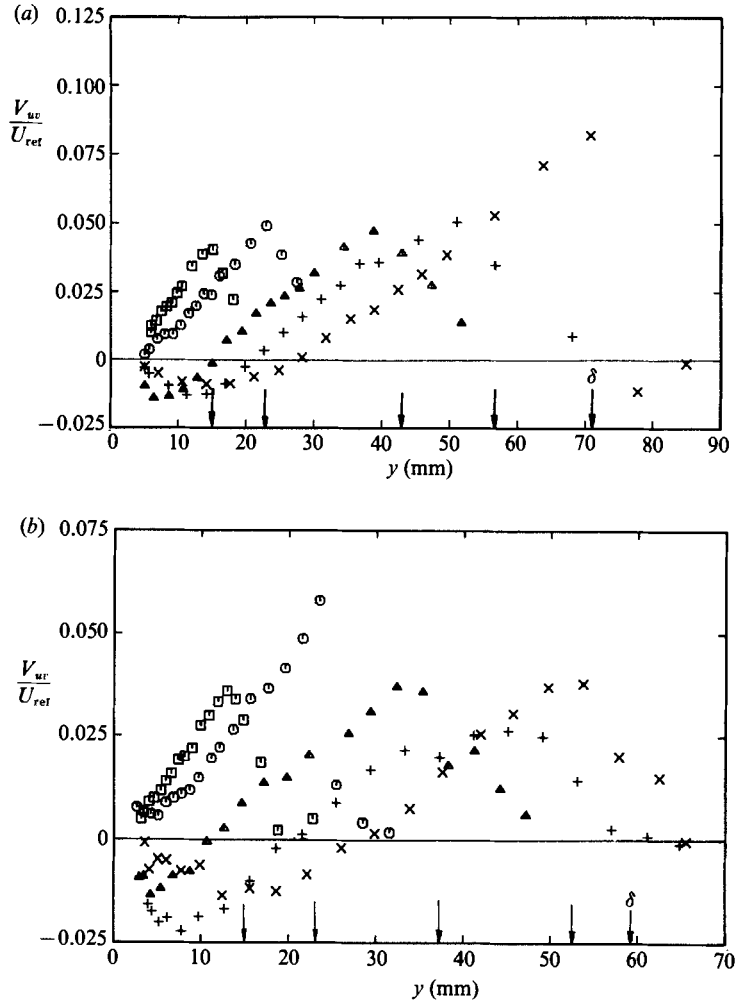

FIGURE 16. Transport velocity of $-\overline{uv}$ normal to the surface. (*a*) Concave curvature. (*b*) Convex curvature.

and their ratio is denoted as

$$N_e = \nu_{cm}/\nu_{sm} = \tan\phi_{\tau m}/\tan\phi_{gm},$$

where the shear stress components are also referred to the coordinates aligned to the local mean flow, as denoted by the suffix 'm'. ϕ_{gm} and $\phi_{\tau m}$ are respectively the directions of the resultant mean velocity gradient and resultant shear stress vectors with respect to the local mean flow. Many experiments on three-dimensional shear layers on a flat surface (e.g. Johnston 1976), however, have shown that the directions of the velocity gradient and shear stress vectors are different ($N_e \neq 1$), contradicting the assumption of isotropic eddy viscosity for closure purposes. Nevertheless, by far the majority of the prediction methods used in industry and government laboratories use this assumption. It is not even meaningful to use the local mean flow direction as an axis, since turbulence properties and velocity gradients are translationally invariant (i.e. unaltered by adding an arbitrary mean velocity) whereas the flow direction is not; we simply follow common usage. The ratio of the eddy viscosity

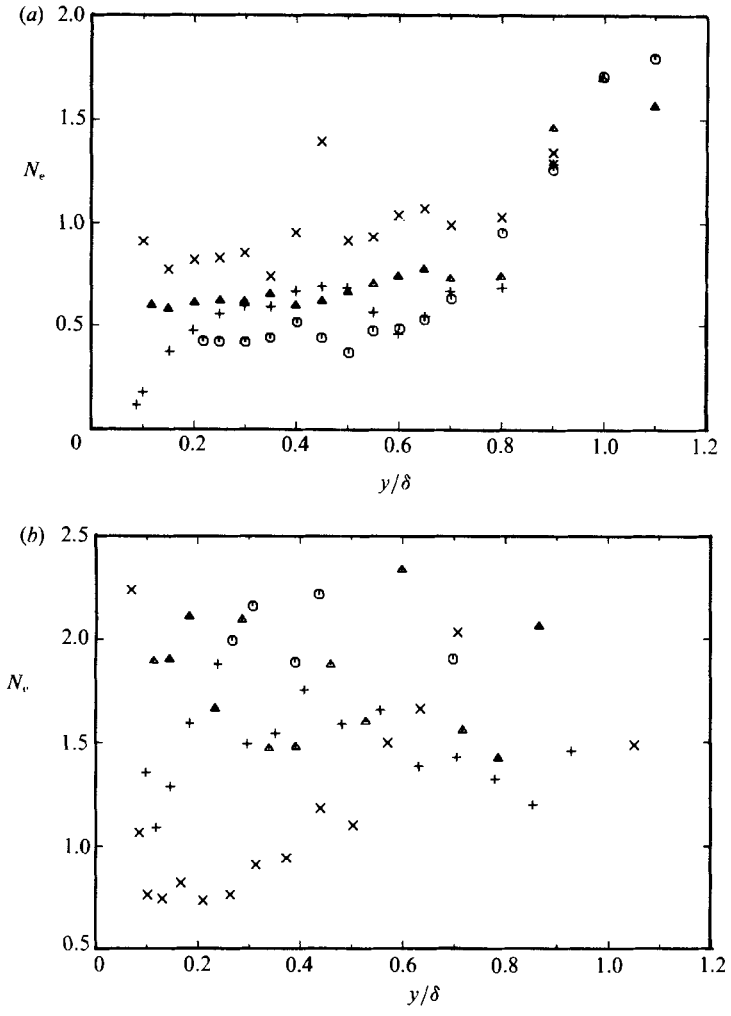

FIGURE 17. Ratio of the eddy viscosity components. (*a*) Concave curvature; (*b*) Convex curvature.

components is shown in figure 17 for the two curved flow cases. $N_e < 1$ over the concave wing, indicating that the shear stress lags behind the velocity gradient as in the flat-wing case of Bradshaw & Pontikos, and in the convex case $N_e > 1$ which corresponds to a lead of shear stress over the velocity gradient. In both cases, an isotropic eddy viscosity is inadequate to predict the flow. This implication also holds for an isotropic mixing length. The tendency of N_e to approach unity in both cases at the last measurement station is due to the relaxation of pressure gradient from adverse to favourable, and is a genuine indication that the three-dimensional boundary layer is pressure driven.

The calculation of Bradshaw, Mizner & Unsworth as applied to the present curved-wing flows needs some comment. Using this method in the case of Bradshaw & Pontikos, the skin friction coefficient was overestimated by 20%. Poor prediction of C_f is not surprising since the method does not allow for the change in the structure due to crossflow: for example, it uses the two-dimensional empirical value of 0.15 for the ratio of the shear stress to the turbulent kinetic energy. Therefore the good

agreement with the present concave-wing data could be a coincidence, even though the calculation produces results consistent with the idea of superposition of crossflow and concave curvature effects. The nonlinear interaction between the two effects, and poor agreement with calculation, in the convex case certainly supports the finding that concave and convex effects are qualitatively different in two-dimensional curved wall boundary layers. More experiments on three-dimensional boundary layers involving streamline curvature are needed to substantiate the difference in the behaviour depending on the sense of curvature

5. Conclusions

Measurements were made in three-dimensional layers in test rigs simulating 'infinite' swept curved wings with concave and convex surface curvature. The chordwise crossflow distributions were simulated to be approximately the same as in the 'infinite' flat wing of Bradshaw & Pontikos (1985). The curvature parameter, δ/R, is typical of values used in the earlier two-dimensional curved flow studies of Hoffmann *et al.* (1985) with concave curvature, and of Muck *et al.* (1985) with convex curvature. Combined crossflow and mild curvature of either sign have little net effect on the turbulence structure, in contrast to the large influence of each when applied individually. This suggests that the stabilizing effect of crossflow opposes the destabilizing influence of concave curvature. In contrast, the weak influence of convex curvature and crossflow together suggests a nonlinear interaction. In both curved flow cases, the different directions for the mean velocity gradient vector and the shear stress vector imply that hypotheses based on isotropic eddy viscosity or mixing length are inadequate. The calculation method of Bradshaw, Mizner & Unsworth, a simple shear-stress transport model, gives good predictions in the case of concave curvature, but agreement in the flat-surface case is poor and in the convex-curvature case it is even poorer. The method does not account for the effects of crossflow on the turbulence structure so that the absolute level of agreement is expectedly poor, but the trend supports the superposition principle for concave surfaces. More experiments are needed on curved three-dimensional boundary layers of either sign, with different values for the radius of curvature, to confirm and to extend the findings of the present experiments.

We gratefully acknowledge the support received from the Ministry of Defence, Procurement Executive, monitored by Mr M. C. P. Firmin of the Royal Aerospace Establishment, and we are grateful to Dr P. D. Smith of the Royal Aerospace Establishment for his comments on the three-hole yawmeter behaviour close to the wall. We thank the referees for their constructive criticism.

REFERENCES

ANDERSON, S. D. & EATON, J. K. 1987 An experimental investigation of pressure driven three-dimensional turbulent boundary layers. *Stanford Univ. Thermosci. Divn Rep.* MD-49.

BARLOW, R. S. & JOHNSTON, J. P. 1988 Structure of a turbulent boundary layer on a concave surface. *J. Fluid Mech.* **191**, 137.

BASKARAN, V. & BRADSHAW, P. 1987 Experimental investigation of a three-dimensional turbulent boundary layer on an 'infinite' swept concave wing. *Imperial College of Sci. & Tech., Dept of Aeronautics, Final Contract Rep.* MoD(PE) Agreement AT/2037/0243.

BASKARAN, V. & BRADSHAW, P. 1988 Decay of spanwise wavy inhomogeneities in a three-dimensional boundary layer over an 'infinite' swept concave wing. *Expt. Fluids* **6**, 487.

BASKARAN, V., PONTIKIS, Y. M. & BRADSHAW, P. 1987 Experimental investigation of a three-dimensional boundary layer over an 'infinite' swept convex wing. *Imperial College of Sci. & Tech., Dept of Aeronautics, Final Contract Rep.* MoD(PE) Agreement AT/2037/0243.

BASKARAN, V., SMITS, A. J. & JOUBERT, P. N. 1987 Turbulent flow over a curved hill. Part 1. Growth of an internal boundary layer. *J. Fluid Mech.* **182**, 47.

BERG, B. VAN DEN, ELSENAAR, A., LINDHOUT, J. P. F. & WESSELING, P. 1975 Measurements in an incompressible three-dimensional turbulent boundary layer under infinite swept conditions, and comparison with theory. *J. Fluid Mech.* **70**, 127.

BRADSHAW, P. 1971*a* Calculation of three-dimensional boundary layers. *J. Fluid Mech.* **46**, 417.

BRADSHAW, P. 1971*b* *An Introduction to Turbulence and its Measurement.* Pergamon.

BRADSHAW, P. 1987 Turbulent secondary flows. *Ann. Rev. Fluid Mech.* **19**, 53.

BRADSHAW, P., FERRISS, D. H. & ATWELL, N. P. 1967 Calculation of boundary layer development using the turbulent energy equation. *J. Fluid Mech.* **28**, 593.

BRADSHAW, P., MIZNER, G. A. & UNSWORTH, K. 1976 Calculation of compressible turbulent boundary layers on straight-tapered swept wings. *AIAA J.* **14**, 399.

BRADSHAW, P. & PONTIKOS N. S. 1985 Measurements in the turbulent boundary layer on an 'infinite' swept wing. *J. Fluid Mech.* **159**, 105.

BREDERODE, V. DE & BRADSHAW, P. 1976 A note on the empirical constants appearing in the logarithmic law for turbulent wall flows. *Imperial College Aero Rep.* 74–03.

BRYER, D. W. & PANKHURST, R. C. 1971 *Pressure Probe Methods for Determining Wind Speed and Flow Direction.* National Physical Laboratory, HMSO, London.

BUSHNELL, D. M. & MCGINLEY, C. B. 1989 Turbulence control in wall flows. *Ann. Rev. Fluid Mech.* **21**, 1.

COOKE, J. C. & HALL, M. G. 1962 Boundary layers in three-dimensions. *Prog. Aero. Sci.* **2**, 221.

ELSENAAR, A. & BOELSMA, S. H. 1974 Measurements of the Reynolds stress tensor in a three-dimensional turbulent boundary layer under infinite swept wing conditions. *NLRTR* 74095U.

EAST, L. F. 1975 Computation of three-dimensional boundary layers. *FFA TN* AE 1211.

EAST, L. F., SAWYER, W. G. & NASH, C. R. 1979 An investigation of the structure of equilibirium turbulent boundary layers. *Royal Aircraft Establishment, RAE TR* 79040.

FERNHOLZ, H. H. & VAGT, J.-D. 1981 Turbulence measurements in an adverse-pressure-gradient three-dimensional boundary layer along a circular cylinder. *J. Fluid Mech.* **111**, 233.

GILLIS, J. C. & JOHNSTON, J. P. 1983 Turbulent boundary-layer flow and structure on a convex wall and its redevelopment on a flat plate. *J. Fluid Mech.* **135**, 123.

HALL, P. 1984 The Görtler vortex instability mechanism in three-dimensional boundary layers. *NASA CR* 172370.

HOFFMANN, P. H., MUCK, K. C. & BRADSHAW, P. 1985 The effect of concave surface curvature on turbulent boundary layers. *J. Fluid Mech.* **161**, 371.

JOHNSTON, J. P. 1970 Measurements in a three-dimensional boundary layer induced by a swept forward facing step. *J. Fluid Mech.* **42**, 823.

JOHNSTON, J. P. 1976 Experimental studies in three-dimensional turbulent boundary layers. *Stanford Univ. Thermosci. Divn Rep.* MD-34.

MUCK, K. C., HOFFMANN, P. H. & BRADSHAW, P. 1985 The effect of convex surface curvature on turbulent boundary layers. *J. Fluid Mech.* **161**, 347.

PATEL, V. C. 1965 Calibration of the Preston tube and limitations on its use in pressure gradients. *J. Fluid Mech.* **23**, 185.

PIERCE, F. J. & ZIMMERMAN, B. B. 1973 Wall shear stress inference from two- and three-dimensional boundary layer velocity profiles. *Trans. ASME* I: *J. Fluids Engng.* **95**, 61.

SMITS, A. J. & WOOD, D. H. 1985 Perturbed turbulent boundary layers. *Ann. Rev. Fluid Mech.* **17**, 321.

TANI, I. 1962 Production of longitudinal vortices in the boundary layer along a concave wall. *J. Geophys. Res.* **67**, 3075.